RSC
Chemical Biology

ROYAL SOCIETY
OF CHEMISTRY

PAPER

View Article Online
View Journal | View Issue

Check for updates

Cite this: *RSC Chem. Biol.*, 2022, **3**, 905

RT-qPCR as a screening platform for mutational and small molecule impacts on structural stability of RNA tertiary structures†

Martina Zafferani, Dhanasheel Muralidharan, Nadeska I. Montalvan and Amanda E. Hargrove*

Received 18th January 2022,
Accepted 25th May 2022

DOI: 10.1039/d2cb00015f

rsc.li/rsc-chembio

The exponential increase in the discovery and characterization of RNA tertiary structures has highlighted their active role in a variety of human diseases, yet often their interactome and specific function remain unknown. Small molecules offer opportunities to both decode these cellular roles and develop therapeutics, however there are few examples of small molecules that target biologically relevant RNA tertiary structures. While RNA triple helices are a particularly attractive target, discovery of triple helix modulators has been hindered by the lack of correlation between small molecule affinity and effect on structural modulation, thereby limiting the utility of affinity-based screening as a primary filtering method. To address this challenge, we developed a high-throughput RT-qPCR screening platform that reports on the effect of mutations and additives, such as small molecules, on the stability of triple helices. Using the 3′-end of the oncogenic long non-coding RNA MALAT1 as a proof-of-concept, we demonstrated the applicability of both a two-step and a one-pot method to assess the impact of mutations and small molecules on the stability of the triple helix. We demonstrated the adaptability of the assay to diverse RNA tertiary structures by applying it to the SARS-CoV-2 pseudoknot, a key viral RNA structure recently identified as an attractive therapeutic target for the development of antivirals. Employment of a functional high-throughput assay as a primary screen will significantly expedite the discovery of probes that modulate the structural landscape of RNA structures and, consequently, help gain insight into the roles of these pervasive structures.

Introduction

Advances in biophysical techniques aimed at studying RNA structure have resulted in an exponential increase in discovery and characterization of RNA tertiary structures.[1,2] For example, the recent surge in interest and characterization of RNA triple helices across various kingdoms of life has led to coining of the term 'triplexome', referring to the diverse and large number of RNA triple helices involved in cellular processes.[3] While many of the functions of triplexome members are still being elucidated, the recognized roles of this RNA structural topology include protection of RNA from degradation, protein recruitment, and nuclear localization.[4–7] RNA triple helices have been found in a variety of long non-coding RNAs, and the structuredness of the triplex motif has been shown to render the transcript refractory to exonuclease degradation, ultimately promoting its cellular accumulation.[3–5,8] Despite the continuous increase in the size of the triplexome, small molecule targeting of these structures has significantly lagged, with only a few examples published.[9–11] Notably, recent studies showed that small molecule modulation of RNA structure and function cannot always be predicted by affinity alone, highlighting the need for more cost efficient high-throughput assays that report on the effects of small molecule:RNA interactions in relationship to structural stability.[12] Furthermore, affinity-based screening platforms for RNA tertiary structures are limited due to the inherent challenges of optimizing binding assays for larger, more complex structures.[12] Function-based assays would help bridge the gap between *in vitro* screening and biological activity, thereby expediting the discovery of small molecule modulators for the continuously growing number of RNA tertiary structures such as triple helices. In turn, affordable high-throughput screening platforms can enable researchers to screen both mutations and small molecules and assess their impact on RNA structural stability, ultimately providing essential insight into the role of complex RNA structures in disease pathways.

Methodologies commonly employed to assess RNA structural stability include circular dichroism (CD), UV absorbance

---

Department of Chemistry, Duke University, 124 Science Drive, Durham, NC 27705, USA. E-mail: amanda.hargrove@duke.edu

† Electronic supplementary information (ESI) available. See DOI: **https://doi.org/10.1039/d2cb00015f**

spectroscopy (UV-Vis), differential scanning calorimetry (DSC), and differential scanning fluorimetry (DSF).[13–16] While CD and UV-Vis can provide a variety of thermodynamic parameters, they suffer from low throughput and generally require large amounts of RNA, severely limiting their scope and application to sizeable screenings. DSC and DSF can be optimized for high-throughput screening and can provide information on the impact of a variety environmental factors on RNA structure, but the use of heat can lead to results that do not reflect an output relevant to biological environments.[16] Furthermore, while DSC and DSF can readily identify molecules with thermal stabilizing effects, the identification of molecules with destabilizing effects is rare. Finally, recent developments and optimization of RNA enzymatic degradation assays have shown them to be uniquely poised to interrogate the effect of additives on RNA structural stability and resistance to enzymatic degradation in a more biologically relevant setting.[9,10] However, enzymatic degradation assays are often analyzed through gel electrophoresis and are thus severely limited both in throughput and quantitative potential. It is imperative to develop high-throughput methodologies that assess the effect of small molecules and other additives on RNA structure reliably, quickly, and cost-effectively under biologically relevant conditions.

While the link between structural stability of RNA triplexes and their biological function is a relatively recent discovery, the stability-function relationship is a well-established relationship for frameshifting pseudoknots and RNA G-quadruplexes (rG4s), making them a good reference for our functional assay.[17] For example, highly stable rG4s can result in a premature stop in ribosomal scanning and prevent translation of the mRNA transcript downstream.[17] Similarly, rG4s stability leads to stalling of reverse transcriptases and premature termination of reverse transcription, an outcome that has been recently used to map the presence of rG4s across the transcriptome.[18,19] This finding led to the preliminary investigation of quantitative PCR (qPCR) on the reverse transcribed cDNA template as a potential method to identify G-quadruplex structures.[20,21] Recently, Katsuda and co-workers were able to employ this method in a screen to identify small molecules that increased the stability of RNA G-quadruplexes by observing their effect on the length and amount of cDNA formed during reverse transcription of the RNA.[22] The small molecule identified as an inhibitor of the elongation reaction of the reverse transcriptase (RT) in the mRNA TERRA was also confirmed as a translation inhibitor *in cellulo*, corroborating the biological relevance of the *in vitro* RT assay.[22] Based on the success of this method in identifying functional modulators of a G-quadruplex, we sought to ask whether an RT-qPCR reaction could be optimized for application in a general cost-effective high-throughput platform for RNA tertiary structural stability. In addition to the use of a two-step method and high input of RT in the previous experiments, the reported structuredness and thermal stability of RNA G-quadruplexes brings into question whether this assay can be optimized and applied to more complex and/or less stable RNA tertiary structures.[22] We also aimed to assess whether an RT-qPCR method could identify both stabilizing and destabilizing mutations and small molecules. We hypothesized that such an assay could both elucidate key interactions necessary for triplex formation and stability *via* mutant analysis and provide useful modulators to facilitate elucidation of triplex-mediated regulatory pathways to unravel new potential therapeutic avenues.

To ensure the applicability and biological relevance of the newly developed high-throughput RT-qPCR screening platform presented herein, we chose the well-studied MALAT1 triple helix as our initial proof-of-concept. The A-U rich blunt-ended MALAT1 triple helix forms at the 3′-end of a 6.7 kb long non-coding RNA (lncRNA) found to be overexpressed in several types of cancers and implicated in a variety of human diseases, including diabetes.[23,24] While the structure and functions of the entire transcript are still under investigation, the triple helix has been reported as essential for protection of the transcript from enzymatic degradation, ultimately leading to increased cellular accumulation of MALAT1.[24,25] Indeed, knockdown of MALAT1 in small cell lung adenocarcinoma mouse models led to significant decrease in tumor size and metastasis, confirming the oncogenic role of this lncRNA.[26] Biophysical studies by Steitz and co-workers further showed that mutations aimed at destabilizing the triple helix structure led to a significant depletion of MALAT1 *in cellulo*, establishing the modulation of the MALAT1 triplex as a potential therapeutic avenue.[24] To further probe the general applicability of the assay to RNA tertiary structures of biological relevance, we adapted this method to an RNA tertiary structure within the SARS-CoV-2 genome.[27] Specifically, the SARS-CoV-2 frameshifting pseudoknot has been highlighted as an essential structure for programmed ribosomal frameshifting to occur.[28,29] This process is a common strategy amongst viruses that allows the pathogen to increase the coding potential of its genome by translating two overlapping reading frames (ORFs) and, consequently, control the expression of structural and non-structural viral proteins at different stages of viral lifecycle.[30] Consequently, the application of the RT-qPCR assay to this recently discovered RNA structure revealed that two recently found frameshifting inhibitors result in stabilization of the SARS-CoV-2 pseudoknot, thus providing a new stability-centric platform to discover small molecule modulators and expedite RNA-targeted antiviral development.

Results and discussion

Assay and MALAT1 construct design

The 3′-MALAT1 triple helix forms *via* recruitment of a genomically encoded A-rich tail to the adjacent U-rich region after processing of the full-length transcript.[31] Given the critical function and sequestration of the 3′-end, we sought to avoid the use of an A-tail specific reverse primer for the reverse transcription reaction to retain its ability to form a triplex structure. We thus synthesized a construct containing a primer handle commonly used in chemical probing experiments (SHAPE cassette, Fig. 1, orange).[32,33] Indeed, SHAPE cassettes have been successfully employed in chemical probing experiments of MALAT1 and MALAT1-like evolutionarily conserved

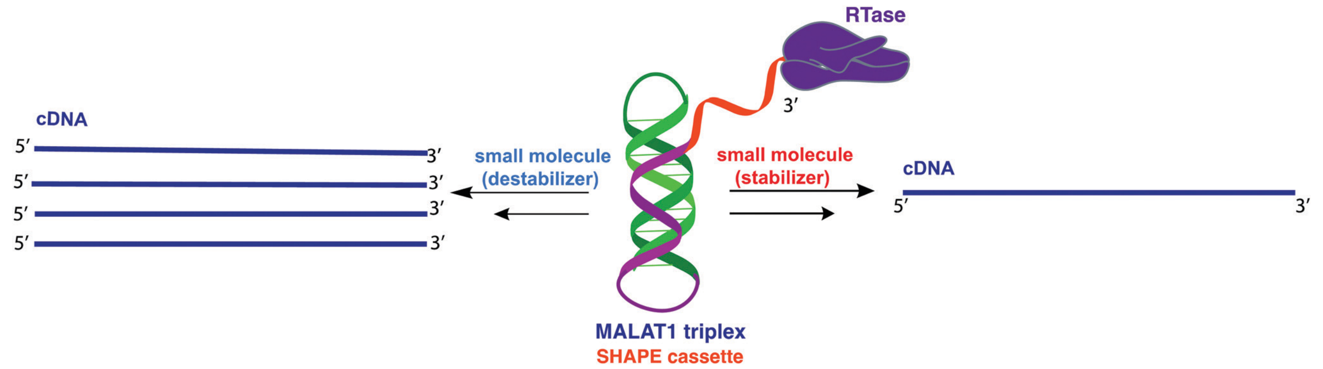

Fig. 1 Schematic representation of small molecule-induced structural modulation of the MALAT1 triple helix assessed *via* RT-qPCR assay. The MALAT1 triple helix (green/purple) is equipped with a structural SHAPE cassette (orange) to prevent competition between primer binding and triplex formation. According to the assay design, small molecules that destabilize the triple helix construct result in lower frequency of RT stalling and, consequently, in more full-length cDNA synthesis (left). Small molecules that stabilize the triple helix structure result in higher occurrence of RT stalling, ultimately resulting in lower amounts of full cDNA synthesis (right). Reverse transcription reactions are then followed by qPCR for quantification (not shown).

transcripts, and the results were consistent with triple helix formation (Fig. S1, ESI†).[34] In the system designed here, small molecules that stabilize the triple helix will result in inhibition of the reverse transcription reaction due to the inability of the chosen RT enzyme (SuperScript IV, ThermoFisher) to unwind structured regions. Inhibition of the elongation reaction will ultimately result in lower levels of cDNA produced, which can be measured quantitatively *via* qPCR and expressed as cycle threshold (C_t), values (Fig. 1). Analogously, small molecules that destabilize the triple helix conformation will enable for more efficient readthrough of the RT, yielding higher cDNA and a resulting lower C_t value than the control (Fig. 1). Specifically, C_t value is the number of cycles needed during qPCR for the fluorescent signal of the dye (two-step RT-qPCR) or the FRET probe (one-pot RT-qPCR) to exceed a set threshold above background signal. Thus, the C_t value is inversely proportional to the amount of target cDNA present in the sample and, consequently, to the efficiency of reverse transcription.[35]

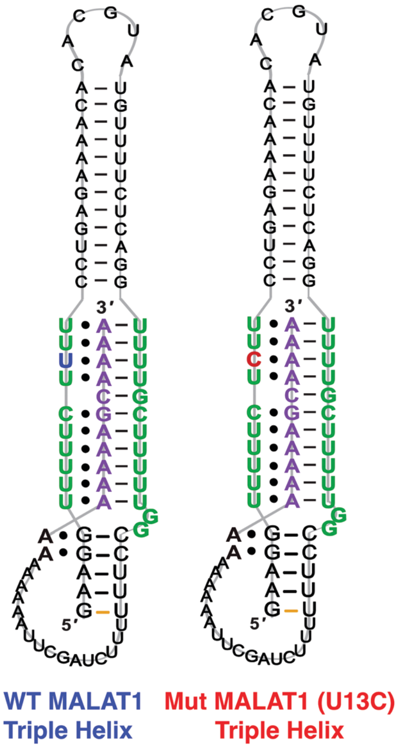

Fig. 2 2D structure and sequence of MALAT1 WT and U13C mutant.

Upon successful synthesis of the designed MALAT1 construct (Table S1 and Fig. S1, ESI†), we first optimized the assay for the evaluation of mutational effects on structural stability, particularly destabilizing effects. Accordingly, we synthesized a construct containing a MALAT1 mutant where one of the uracils involved in a base triple within the triplex core is mutated to a cytosine (U13C). This U13C mutant was reported by Steitz and co-workers as a triplex destabilizing mutation that resulted in a decrease of full-length MALAT1 levels *in cellulo* (Fig. 2).[24]

Two and one-step RT-qPCR

A two-step RT-qPCR was first utilized to allow for optimization of the reverse transcription and qPCR steps independently. The MALAT1 wild type (WT) and mutant (U13C) were incubated with DMSO control at room temperature after which reverse transcriptase (SSIV), magnesium, primers, and dNTPs were added on ice. The reverse transcription reaction was then carried out at 37 °C, the optimal temperature for the activity of the enzyme, and inactivated by heating to 98 °C after 15 minutes from the start of the reaction. The reaction was then aliquoted in a 96-well light cycler plate and qPCR mix was added to each well and placed in a real-time qPCR machine for cDNA amplification (Fig. 3(A)). Both reverse transcription and qPCR steps were optimized to obtain WT amplification with a C_t that would allow detection of $\Delta\Delta C_t = \pm 4$ without exceeding the instrument detection limit (<2 C_t) or incurring non-specific amplification (>25 C_t).[36] Detection of $\Delta C_t = \pm 2$ corresponds to a 75% change in RT efficiency.[22] Initial RNA quantities were in line with manufacturer recommendations. The reverse transcription reaction was optimized by testing

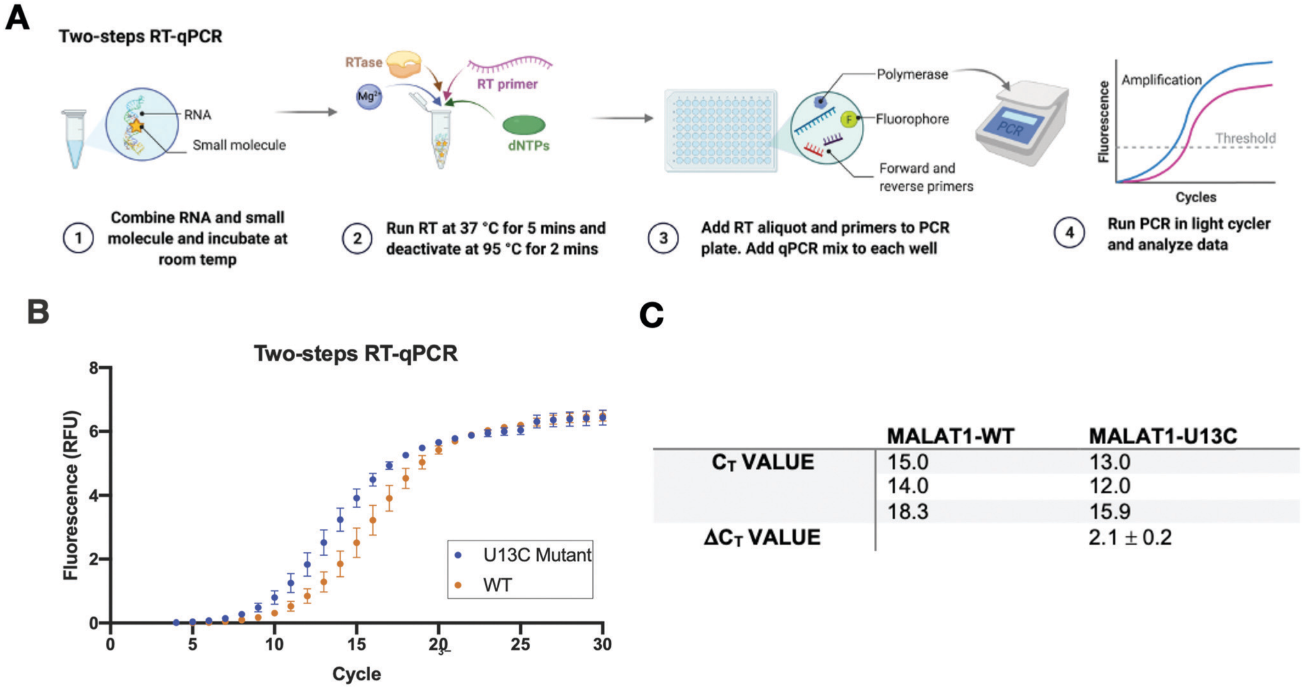

	MALAT1-WT	MALAT1-U13C
C_T VALUE	15.0	13.0
	14.0	12.0
	18.3	15.9
ΔC_T VALUE		2.1 ± 0.2

Fig. 3 Two-step RT-qPCR system. (A) Schematic of the two-step RT-qPCR reaction with the reverse transcription reaction being performed in a thermocycler and then being aliquoted in a 96-well plate for qPCR amplification, which is performed in a light cycler. (B) Amplification curves obtained from 3 independent replicates of RT-qPCR of the U13C MALAT1 mutant and the WT triple helix. Error bars are standard deviation calculated over the three independent experiments. (C) C_t values calculated over three independent experiments for WT and U13C mutant (ΔC_t value = $C_{t\,WT} - C_{t\,Mut}$). The mutated destabilized construct amplifies faster than the WT, in agreement with trends reported by Steitz and co-workers.

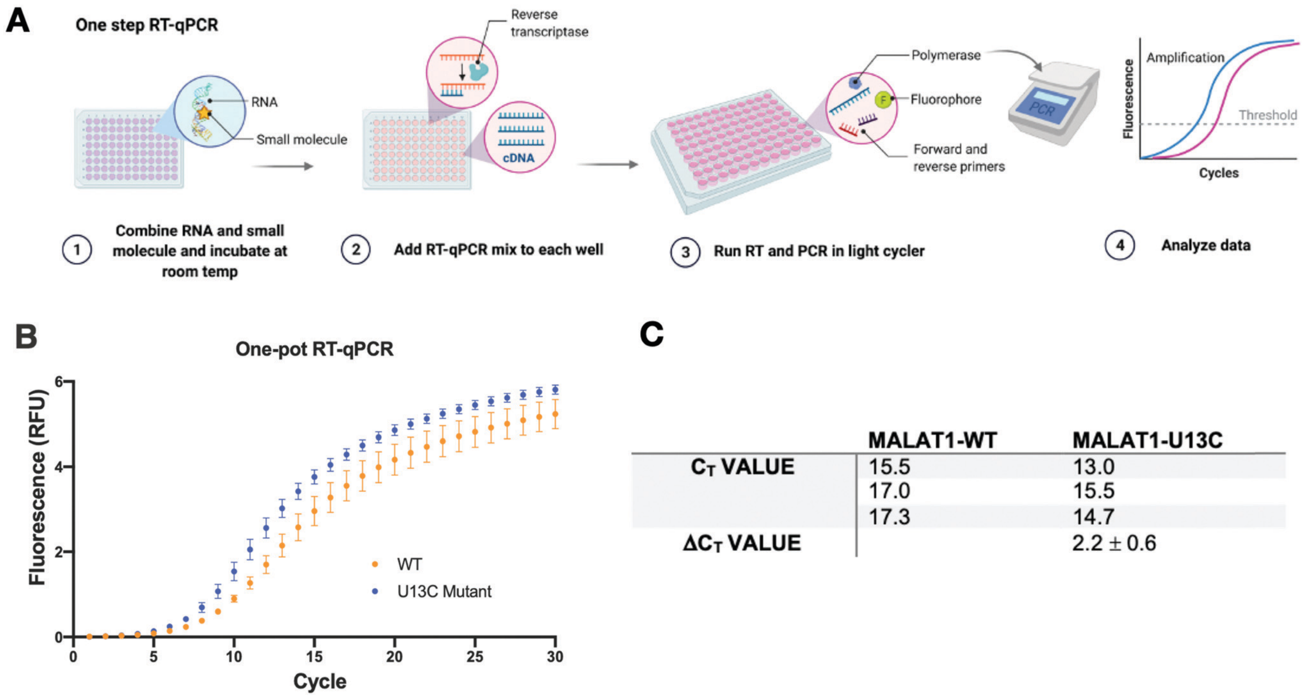

	MALAT1-WT	MALAT1-U13C
C_T VALUE	15.5	13.0
	17.0	15.5
	17.3	14.7
ΔC_T VALUE		2.2 ± 0.6

Fig. 4 One pot RT-qPCR system. (A) Schematic of the one-pot RT-qPCR reaction with reverse transcription reaction being performed in a 96-well format in a light cycler instrument. (B) Raw data obtained from 3 independent replicates of RT-qPCR of the U13C MALAT1 mutant and the WT triple helix. Error bars are standard deviation calculated over the three independent experiments. (C) C_t values obtained for the Mut and WT constructs (ΔC_t value = $C_{t\,WT} - C_{t\,Mut}$). The mutated destabilized construct amplifies faster than the WT, in agreement with trends reported by Steitz and co-workers.

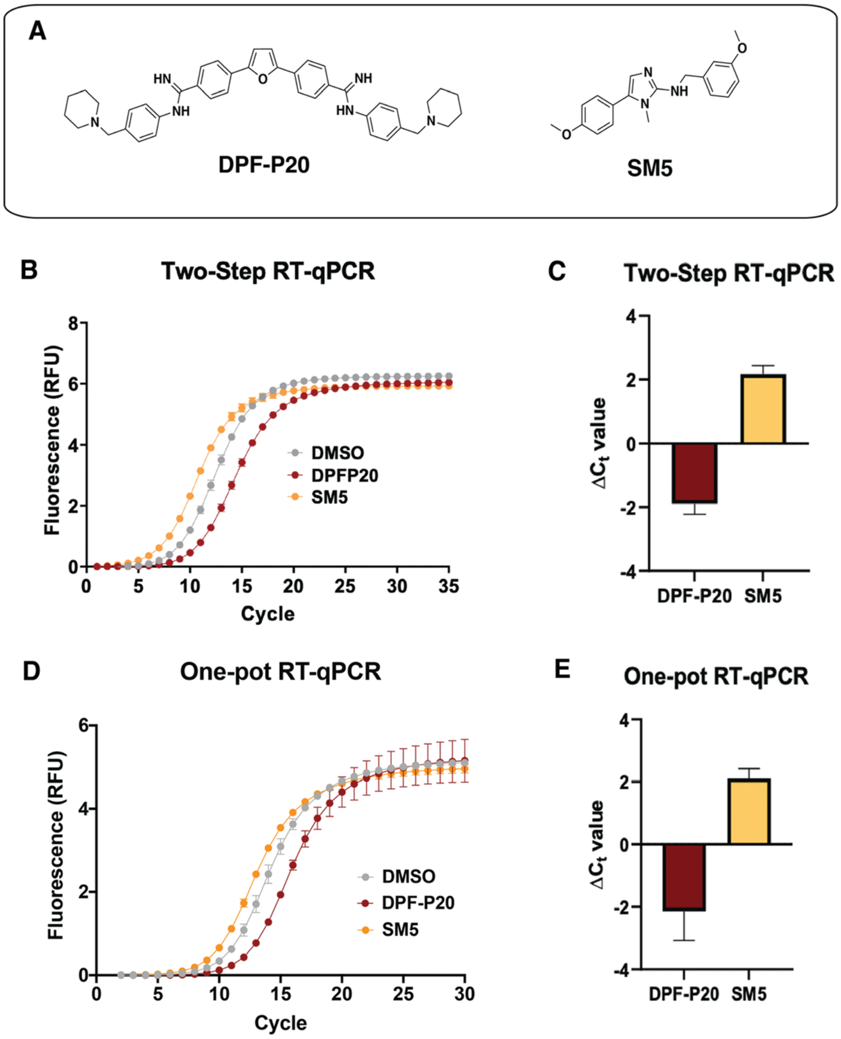

Fig. 5 Application of RT-qPCR assays to assess small molecule effect on MALAT1 WT triple helix stability. (A) Structures of two small molecules chosen for assay validation. Both **DPF-P20** (a MALAT1 triplex stabilizer) and **SM5** (a MALAT1 triplex destabilizer) were previously evaluated in relationship to their effect on triplex enzymatic degradation.[9,10] (B) Raw data obtained for the two-step RT-qPCR procedure for both small molecules. (C) Small molecule ΔC_t values calculated in reference to DMSO (ΔC_t value = $C_{t\,\text{DMSO}} - C_{t\,\text{SM}}$) from 4 independent replicates are in agreement with their reported effect on MALAT1 triplex enzymatic degradation. (D) Raw data obtained for the one-pot RT-qPCR procedure for both small molecules. (E) Small molecule ΔC_t values calculated in reference to DMSO (ΔC_t value = $C_{t\,\text{DMSO}} - C_{t\,\text{SM}}$) from 4 independent replicates in reference to DMSO are in agreement with their reported effect on MALAT1 triplex enzymatic degradation and in line with the values obtained in the two-step RT-qPCR procedure. All error bars represent the standard deviation calculated over the four independent experiments.

whether the reaction needed the presence of ''first-strand buffer'' for reverse transcription (1 M DTT, 0.5 M tris–HCl, 0.25 M KCl, at pH 8.0). Two reverse transcription reactions were carried out in small scale (20 μL) with first strand buffer or water and the reaction was quenched and cleaned up after 30 minutes at 37 °C. The presence of cDNA was assessed by Agarose gel and by Nanodrop, which qualitatively showed equal amounts of cDNA in both reactions. Given the presence of denaturant and the non-biologically relevant pH of the first strand buffer, the RT reaction was subsequently optimized without first strand buffer. Subsequent optimization included variation of reverse transcriptase amount (Thermo Fisher, 30–150 units), magnesium chloride concentration (1–7.5 nM), reverse primer concentration (150–500 nM), dNTP concentration (100–600 nM), and RNA concentration (10–15 nM). After successful optimization of the reverse transcription reaction (final conditions: 15 SSIV units, 10 nM of RNA, 150 nM of primers, 600 nM of dNTPs, 300 nM of $MgCl_2$), qPCR (KAPA) was optimized by varying the amount of cDNA added to the mix (1–3 μL of a max 200 ng μL^{-1} RT reaction). Analysis of the qPCR curve yielded a lower C_t value for MALAT1-U13C when compared to the MALAT1-WT, ultimately yielding a $\Delta C_t = 2.1 \pm 0.2$ (Fig. 3(B) and (C)).

Having optimized a two-step reaction, the MALAT1 WT and Mut were analogously employed in a one-pot RT-qPCR kit (QuantaBio), which would enable cost-efficient, high-throughput screening of additives and small molecules. In this system, both the reverse transcription and the qPCR amplification are performed directly in a real-time qPCR instrument (Fig. 4(A)). The one-pot reaction was optimized by varying the RNA concentration in the reaction (1–20 nM) and the forward and reverse primer concentration (200–500 nM) in the same buffer previously used to obtain C_t values in the same range as the two-step RT-qPCR optimized above. Once again, we found that the MALAT1 mutant has lower C_t value than the wild type, yielding a $\Delta C_t = 2.2 \pm 0.6$ (Fig. 4(B) and (C)). In summary, both methodologies were confirmed to report on mutation-induced changes in MALAT1 triplex structural stability and, most importantly, were consistent with the trends Steitz and co-workers observed in a cellular environment.

Small molecule screening against the MALAT1 triple helix

Next, we tested the applicability of both RT-qPCR routes to evaluate the impacts of small molecules on the MALAT1 WT triple helix. For this purpose, we chose two previously published small molecules that have been classified as stabilizers or destabilizers, respectively (Fig. 5(A)).[9,10]

DPF-P20 has been recently reported as a MALAT1 triple helix stabilizers as it increases the triplex thermal stability measured *via* DSF as well as inhibits RNase R-mediated exonucleolytic degradation of the triplex (Fig. 5(A)).[9] Both the two-step and the one-pot method identified **DPF-P20** as a triplex stabilizer, yielding less cDNA and higher C_t values than the DMSO control ($\Delta C_{t(2\text{step})} = -1.9 \pm 0.3$ $\Delta C_{t(1\text{pot})} = -2.3 \pm 0.7$) (Fig. 5(C)–(E)). Recently reported by Le Grice and co-workers, **SM5** was identified as a destabilizer of the MALAT1 triplex resulting in reduction of MALAT1 accumulation in *ex vivo* organoid breast cancer models (Fig. 5(A)).[10] **SM5** has also been shown by Donlic and co-workers to increase RNase R-mediated exonucleolytic degradation of the triple helix over time.[9] In line with previous studies, **SM5** resulted in lower C_t values than the DMSO control, confirming its triplex destabilizing properties ($\Delta C_{t(2\text{step})} = 2.2 \pm 0.3$ $\Delta C_{t(1\text{pot})} = 2.1 \pm 0.3$) (Fig. 5(B) and (C)). ΔC_t values were in the same range in both the two-step and the one-pot RT-qPCR method, showcasing the consistency and applicability of both approaches. (Fig. 5(D) and (E)). As expected, given the sensitivity of RT-qPCR, *Z*-factor control experiments for the one-pot method were suitable for a high-throughput screening platform (*Z*-factor = 0.93, Fig. S3, ESI†). The $|\Delta C_t|$ values observed for the MALAT1 triplex modulators are comparable to the values obtained by Katsuda and co-workers for the best identified leads of G-quadruplex stabilizers. The authors used $\Delta C_t \geq 2$ as a cutoff for lead molecules since a value of 2 corresponded to a 75% decrease in RT elongation.[22] Both small molecules, **DPF-P20** and **SM5**, would be classified as hits under these conditions, and we propose the same cutoff for the assay reported here. For promising small molecule stabilizers, it will be important to rule out possible interference from small molecule inhibition of the RT or polymerase enzymes, which can be accomplished in complementary or secondary assays.

Application of RT-qPCR assay to functional RNA elements in SARS-CoV-2 genome

Viral protein expression is finely tuned by a tertiary structure element at the interface of two overlapping open reading frames (ORF) in the SARS-CoV-2 genome.[37–39] The structuredness of this RNA element is known to cause mechanochemical tension in ribosomal elongation, ultimately resulting in stalling and re-positioning in a different frame before continuing

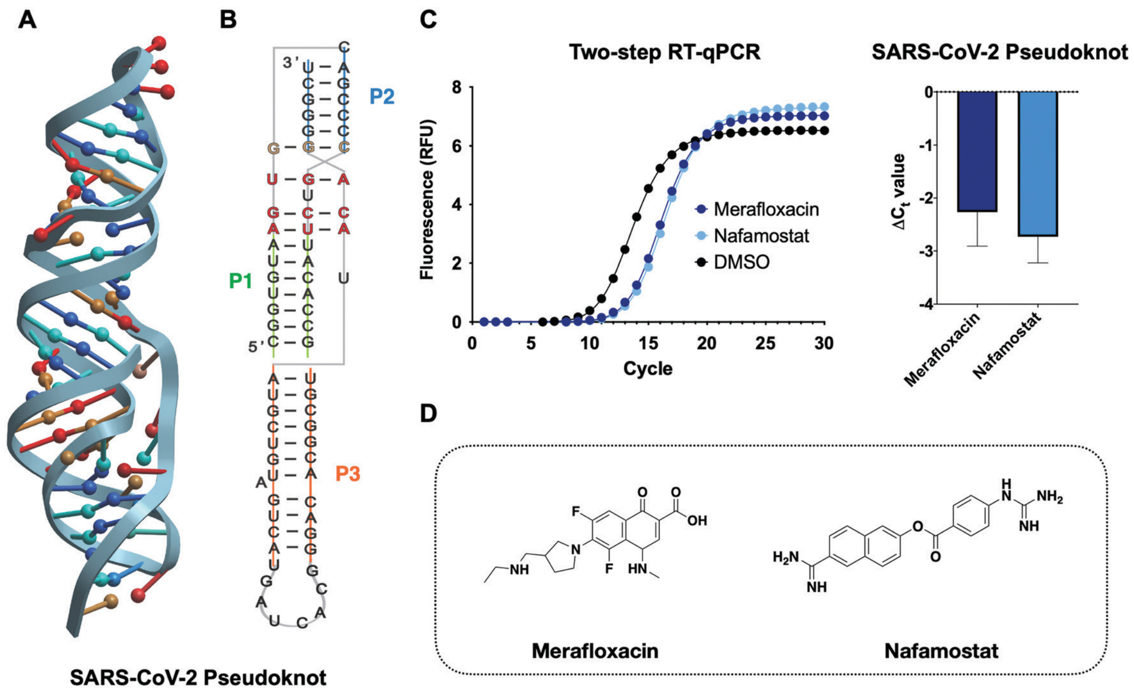

Fig. 6 Application of the RT-qPCR assay to the SARS-CoV-2 pseudoknot. (A) 3D structure of the SARS-CoV-2 frameshifting element pseudoknot structure obtained *via* NMR (PDB: 7LYJ).[28] (B) 2D representation of the pseudoknot and the relative base-pairing according to the structure of D'Amare and co-workers. (C) Chemical structure of two frameshifting inhibitors merafloxacin[29,47] and nafamostat.[48] (D) Two-step RT-qPCR adapted to the SARS-CoV-2 pseudoknot identifies frameshifting inhibitors as stabilizing small molecules.

elongation.[30,40–43] This process, also referred to as programmed ribosomal frameshifting, is essential for viral replication and thus has been identified as a potential antiviral target (Fig. 6).[38,44,45] Consequently, modulating the stability of the RNA pseudoknot can lead to an increase or decrease in frameshifting events, both of which have been shown to lead to viral inhibition. To date, no high-throughput assays have been developed that report on the structural stability of RNA pseudoknots. Indeed, most RNA pseudoknot-focused studies, though limited, resort to *in vitro* or *in cellulo* reporter-based frameshifting assays or biophysical techniques such as Cryo-EM and NMR.[28,46] The reporter-based approach can lead to false positive or false negative results as effects on frameshifting may not reflect engagement of the RNA pseudoknot structure. The structural techniques, on the other hand, are both time- and cost-intensive, thereby preventing its application to sizable screenings. Therefore, the application of the RT-qPCR assay developed herein can significantly expedite the discovery of CoV-2 pseudoknot (CoV-2 PK) binders while providing insight on small molecule recognition of this class of underexplored tertiary structures for which very limited examples have been published to date.

We first aimed to optimize the two-step RT-qPCR assay to the pseudoknot construct alone. Equimolar amounts of CoV-2 PK and MALAT1 triplex input RNA led to faster (lower C_t value) amplification by qPCR for the CoV-2 PK. Optimal C_t values were achieved by decreasing the reverse transcription time and RNA concentrations of the CoV-2 PK. This trend is in agreement with recently reported biophysical characterization of the CoV-2 PK constructs, which displays a shorter region of base triples than MALAT1, potentially impacting its stability in the knotted conformer.[28] Furthermore, frameshifting pseudoknots are known to utilize significant conformational plasticity to control the balance of in-frame *vs.* frameshifted translation. These results suggest that the RT-qPCR platform could, potentially, be employed to gain insight into the differential stability between the two structures.

To benchmark this assay for small molecule screening against the CoV-2 pseudoknot we chose two small molecules recently discovered as frameshifting inhibitors in two separate studies, merafloxacin and nafamostat.[29,47,48] Discovered by Sun and co-workers, merafloxacin was identified through a cell-based luciferase assay in HEK293T cells and was found to inhibit frameshifting and SARS-CoV-2 replication.[49] Nafamostat, on the other hand, was identified in a cell-free luciferase assay as a frameshifting inhibitor of a variety of bat CoVs.[48] Indeed, both studies highlighted the potential of frameshifting elements and, specifically, the SARS-CoV-2 pseudoknot as an attractive therapeutic target to develop mutation-resistant and broad-spectrum antivirals. At the same time, these assays did not inform the relationship between pseudoknot structural stability and inhibition of frameshifting. By screening merafloxacin and nafamostat in our assay, we confirmed direct engagement of the CoV-2 PK target as well as stabilization of the CoV-2 PK as a plausible mechanism of action. Both merafloxacin and nafamostat led to similar levels of stabilization ($\Delta C_{\text{t Meraflox.}} = -2.3 \pm 0.6$ $\Delta C_{\text{t Nafam.}} = -2.7 \pm 0.4$) in our assay, and Munshi and co-workers found similar levels of SARS-CoV-2 frameshifting inhibition between the two molecules, supporting the relevance of this assay for future screening and characterization efforts.[48]

Conclusion

Here, we report the development and optimization of a new high-throughput screening platform that assesses the effects of mutations and small molecule additives on the structural stability of the MALAT1 3′-end RNA triple helix, one of the best studied disease-relevant RNA triple helices. While recent efforts aimed at small molecule targeting and modulation of this RNA motif have identified small molecule binders *via* screening, the effect of the reported small molecules on MALAT1 triplex stability has been studied through low throughput and/or non-biologically relevant techniques.[9,11]

In this work, we developed a high-throughput RT-qPCR screening platform, accessible *via* both two-step and one-pot protocols, utilizing the MALAT1 triple helix and a biologically relevant mutant construct. Robust differences in C_t values of the U13C mutant relative to wild type recapitulated the destabilizing effects of the point mutation, which was previously reported to lead to a decrease of MALAT1 transcript accumulation *in cellulo*. These findings underscored the applicability of this platform to evaluate the effects of mutations on structural stability as well as the likely biological relevance of the trends observed. We then chose two MALAT1 small molecule ligands previously published as stabilizers or destabilizers and evaluated their impacts on the MALAT1 triple helix in both methods. Once again, both approaches resulted in trends consistent with previously published effects of the small molecules on RNase R-mediated exonucleolytic degradation of the triplex. To further highlight the applicability of the assay to other disease-relevant RNA structures we investigated the SARS-CoV-2 frameshifting pseudoknot. We chose two small molecules recently identified in separate studies as frameshifting inhibitors that resulted in a decrease of SARS-CoV-2 replication. Both small molecules were identified as pseudoknot stabilizers, providing first evidence of direct engagement of the SARS-CoV-2 pseudoknot structure and preliminary insight into the relationship between frameshifting inhibition and small molecules' effect on pseudoknot structural stability.

The RT-qPCR-based screening method developed herein establishes a high-throughput platform that can identify RNA-targeted small molecules that have both stabilizing and destabilizing effects on RNA tertiary structure. The ability to identify probes with opposite impacts can greatly help elucidate the many biological roles of RNA tertiary structures such as triple helices and pseudoknots in human disease and expedite the discovery of RNA-targeted therapeutics. Having access to a cost-efficient high-throughput structural stability screening platform can significantly increase the ability to evaluate small molecule selectivity for one structure over another in relationship to structural stability. In turn, the data gathered can help address several unanswered questions such as what molecular properties make a small molecule a stabilizer or a destabilizer and whether we can use structural stability data as a guiding principle for future small molecule design and synthesis. We expect that answering these remaining questions will move the scientific community toward the efficient development of RNA-targeted small molecule therapeutics.

Experimental procedures

Synthesis of the MALAT1 RNA constructs

DNA template sequence was purchased from Dharmacon, and forward and reverse primers were purchased from Integrated DNA technologies (IDT) (Table S1, ESI†). For PCR amplification the following reagents were added for a given 50 μL final reaction volume. First, the entire working space was treated with RNase Zap to prevent contamination. Next, in the desired amount of sterile PCR tubes (ThermoFisher) the reaction's component were adding as detailed in Table 1. The DNA template was then amplified for 30 cycles in an Eppendorf Echo thermocycler. A Zymo DNA-clean-up kit was then utilized to clean up the desired DNA sequence. A solution of amplified DNA in water was made to reach 28–35 ng μL^{-1}. The sequence was then *in vitro* transcribed (IVT) using the protocol detailed in Table 1 per 50 μL reaction.

The reaction was then incubated at 37 °C for 12 hours. Following incubation, the reaction was treated with 2 μL of DNase I (NEB) and 5 μL of DNase I buffer twice in intervals of 30 minutes, followed by addition of 10% of the reaction volume of EDTA. The desired RNA was then extracted using phenol chloroform extraction and further purified *via* ethanol precipitation. Purity and size of the RNA construct was confirmed by Small RNA chip on Agilent Bioanalyzer and 10% TBE denaturing gel (Fig. S2, ESI†).

Table 1 Concentrations and volumes for synthesis of the MALAT1 constructs

	Component	Stock concentration	Volume added (μL)
PCR	Nuclease-free water	N/A	32.5
	Q5 reaction buffer (NEB)	10×	10
	dNTPs	10 mM	1
	Forward primer	10 mM	2.5
	Reverse primer	10 mM	2.5
	DNA template	50 ng μL^{-1}	1
	Q5 polymerase (NEB)	2000 U mL^{-1}	0.5
IVT	Nuclease-free water	N/A	31.75
	$MgCl_2$	1 M	1.25
	Tris–HCl, pH 8.0	1 M	2
	rNTP mix	10 mM	5
	Spermidine	0.1 M	1.25
	Triton-X	0.1%	0.5
	DTT	1 M	0.5
	Pyrophosphatase (NEB)	100 U μL^{-1}	0.2
	DNA from PCR	28–35 ng μL^{-1}	5
	T7 polymerase (Tolbert lab)	50 000 U mL^{-1}	2.5

Table 2 Concentrations and volumes for synthesis of the SARS-CoV-2 pseudoknot

	Component	Stock concentration	Volume added (μL)
PCR	Nuclease-free water	N/A	30
	Q5 reaction buffer (NEB)	10×	10
	dNTPs	10 mM	1
	Forward primer	10 mM	2.5
	Reverse primer	10 mM	2.5
	DNA template	50 ng μL^{-1}	1
	DMSO	N/A	2.5
	Q5 polymerase (NEB)	2000 U mL^{-1}	0.5
IVT	Nuclease-free water	N/A	18.2
	$MgCl_2$	1 M	1
	Tris–HCl, pH 8.0	1 M	4
	rNTP mix	10 mM	3
	Spermidine	0.1 M	1
	DTT	1 M	0.1
	Pyrophosphatase (NEB)	100 U μL^{-1}	0.2
	DNA from PCR	28–35 ng μL^{-1}	10
	T7 polymerase (Tolbert lab)	50 000 U mL^{-1}	2.5
	DMSO	N/A	10

Synthesis of the SARS-CoV-2 RNA pseudoknot constructs

DNA template sequence was purchased from Dharmacon, and forward and reverse primers were purchased from Integrated DNA technologies (IDT) (Table S1, ESI†). For PCR amplification the following reagents were added to for a given 50 μL final reaction volume as detailed in Table 2. First, the entire working space was treated with RNase Zap to prevent contamination.

The DNA template was then amplified for 30 cycles in an Eppendorf Echo thermocycler. A Zymo DNA-clean-up kit was then utilized to clean up the desired DNA sequence. A solution of amplified DNA in water was made to reach 20 ng mL^{-1}. The sequence was then *in vitro* transcribed (IVT) using the protocol detailed in Table 2 for each 50 μL reaction.

The reaction is then incubated at 25 °C for 12 hours. Following incubation, the reaction is then incubated at 37 °C and treated with 3 μL of DNase I (1000 units, NEB) and 6 μL DNase I buffer (NEB) twice in intervals of 30 minutes, followed by addition of 10% of the reaction volume of EDTA. The desired RNA is then extracted using phenol chloroform extraction and the aqueous layer was then subjected to ethanol precipitation. The concentrated product is then re-constituted in 1 mL of water and vortexed to obtain a fully dissolved heterogeneous solution, which is further purified by FPLC (BioRad). The solution is loaded on a 70 SEC column (BioRad) and run *via* isocratic protocol in 50 mM HEPES-KOH, 50 mM KCl, 0.1 mM EDTA at pH 7.5. Purity and size of the RNA construct is confirmed by Small RNA chip on Agilent Bioanalyzer and 10% TBE (Fig. S2, ESI†).

MALAT1 two step RT-qPCR

RNA was synthesized and purified as previously described. For a given reverse transcription reaction RNA was incubated in water with DMSO or small molecules at room temperature for 20 min. After incubation the PCR strip was placed on an ice block. A mastermix of reverse transcription reaction reagents

Table 3 Concentrations and volumes for the two-step RT-qPCR for the MALAT1 triple helix

	Component	Volume added to reaction (μL)	Final concentration
Reverse transcription reaction	DMSO/small molecule	0.8	10 μM
	RNA	4	10 nM
	Reverse primer	3	150 nM
	SSIV	3	15 units
	dNTPs	2.4	600 nM
	$MgCl_2$	0.6	300 nM
	Nuclease free water	26.2	
qPCR reaction	RT reaction	1	
	Reverse primer	0.9	300 nM
	Forward primer	0.9	300 nM
	SYBR mix	10	
	Nuclease free water	17.2	

was prepared and aliquoted in each reaction to reach a total of 40 μL Components were added to the reverse transcription reaction to reach the final concentration listed in Table 3. PCR strip was then incubated at 37 °C in a thermocycler (Eppendorf, Nexus Gradient) for 15 minutes before inactivating the RT enzyme for 5 minutes at 98 °C. The PCR strip was then placed on an ice block. In the meantime, a qPCR mix was prepared according to the concentrations listed in Table 3. The qPCR mastermix was aliquotted in each well of a 96-well lightcycler plate (Roche 96) and 1 μL of RT reaction was added to each. Amplification protocol was run by incubating at 95 °C for 3 minutes followed by a 3-step amplification for 25–45 cycles and a final cooling to 40 °C over the course of 10 minutes. Results were analyzed using the Roche 96 light cycler software v1.1.

SARS-CoV-2 pseudoknot two step RT-qPCR

RNA was synthesized and purified as previously described. The two-step procedure was optimized starting with the conditions used for the MALAT1 triple helix, further showcasing the efficient adaptability of this assay to different RNA structures. For a given reverse transcription reaction RNA was incubated in water with DMSO or small molecules at room temperature for 20 min. After incubation the PCR strip was placed on an ice block. A mastermix of reverse transcription reaction reagents was prepared and aliquoted in each reaction to reach a total of 40 μL Components were added to the reverse transcription reaction to reach the final concentration listed in Table 4. PCR strip was then incubated at 37 °C in a thermocycler (Eppendorf, Nexus Gradient) for 15 minutes before inactivating the RT enzyme for 5 minutes at 98 °C. The PCR strip was then placed on an ice block. In the meantime, a qPCR mix was prepared according to the concentrations listed in Table 4. The qPCR mastermix was aliquoted in each well of a 96-well lightcycler plate (Roche 96) and 1 μL of RT reaction was added to each. Amplification protocol was run by incubating at 95 °C for 3 minutes followed by a 3-step amplification for 25–45 cycles and a final cooling to 40 °C over the course of 10 minutes. Results were analyzed using the Roche 96 light cycler software v1.1.

Table 4 Concentrations and volumes for the two-step RT-qPCR for the SARS-CoV-2 pseudoknot

	Component	Volume added to reaction (μL)	Final concentration
Reverse transcription reaction	DMSO/small molecule	2	25 μM
	RNA	2	3.75 nM
	Reverse primer	3	150 nM
	SSIV	0.5	2.5 units
	dNTPs	2.4	600 nM
	$MgCl_2$	0.6	300 nM
	Nuclease free water	29	
qPCR reaction	RT reaction	1	
	Reverse primer	0.9	300 nM
	Forward primer	0.9	300 nM
	SYBR mix	10	
	Nuclease free water	17.2	

Table 5 Concentrations and volumes for the one-pot RT-qPCR for the MALAT1 triple helix

Component	Volume added to reaction (μL)	Final concentration
Nuclease free water	13	
RNA	5	10 nM
DMSO/small molecule	1	10 μM
Forward primer	2.5	500 nM
Reverse primer	2.5	500 nM
qScript TaqMan	1	1×
1-step SYBR mix	25	1×

One pot RT-qPCR

RNA was synthesized and purified as previously described. For a given RT-qPCR reaction 10 nM of RNA were incubated in water with DMSO or 10 μM of small molecules at room temperature for 20 min in a 96 well lightcycler plate (Roche). During incubation an RT-qPCR mastermix was 1 step SYBR mastermix (QuantaBio), qScript RT enzyme (QuantaBio 1-step RTqPCR kit), and forward and reverse primer solution according to Table 5 for a total of 50 μL for each reaction. The mastermix of reverse transcription reaction reagents was prepared and aliquoted in each well by adding 31 μL of the master mix to each RNA-DMSO or RNA-Small molecule well. The plate was then sealed with optically clear foils and inserted in a Roche 96 light cycler. The RT step was performed by incubating at 37 °C for 10 minutes, followed by an inactivation at 95 °C for 5 minutes. The qPCR step immediately followed with a 3-step amplification carried for 30–35 cycles, which was followed by cooling to 40 °C over the course of 10 minutes. Results were analyzed using the Roche 96 light cycler software v1.1.

Funding

U.S. National Institutes of Health R35 GM124785 (A. E. H.; M. Z.); Research Corporation for Science Advancement COVID Initiative, Award 27340 (A. E. H.; M. Z); Duke University Chemistry Department Burroughs Wellcome Fellowship (M. Z.): Duke University Dean's Summer Research Fellowship (D. M.) Duke University's Biological Sciences Undergraduate Research Fellowship (N. M.).

Conflicts of interest

Nothing to declare.

Acknowledgements

We are grateful to past Hargrove lab members, especially to Dr Emily McFadden and Dr Sarah Wicks, for their feedback and input. We would like to give a special thanks to current members of the Hargrove lab, Marek Zorawski, Justin Martyr, and Emily Swanson, who helped finalized the structure of this manuscript. We are grateful to the Tolbert lab for their generous donation of the T7 polymerase used for *in vitro* transcription. We would also like to thank Dr Jessica Brown for kindly sharing illustrator files to make 2D-renderings of the MALAT1 triple helix and the Duke Biology Department for sharing the use of their Roche light cycler instrument. Figures in this manuscript were made in BioRender.

References

1 A. M. Mustoe, S. Busan, G. M. Rice, C. E. Hajdin, B. K. Peterson, V. M. Ruda, N. Kubica, R. Nutiu, J. L. Baryza and K. M. Weeks, Pervasive regulatory functions of mRNA structure revealed by high-resolution shape probing., *Cell*, 2018, **173**(1), 181–195.e18.

2 J. Sztuba-Solinska, J. W. Rausch, R. Smith, J. T. Miller, D. Whitby and S. F.-J. Le Grice, Kaposi's sarcoma-associated herpesvirus polyadenylated nuclear RNA: A structural scaffold for nuclear, cytoplasmic and viral proteins., *Nucleic Acids Res.*, 2017, **45**(11), 6805–6821.

3 J. A. Brown, Unraveling the structure and biological functions of RNA triple helices, *WIREs RNA*, 2020, **11**(6), e1598.

4 X. Zhang, M. H. Hamblin and K.-J. Yin, The long noncoding RNA Malat1: Its physiological and pathophysiological functions., *RNA Biol.*, 2017, **14**(12), 1705–1714.

5 J. A. West, C. P. Davis, H. Sunwoo, M. D. Simon, R. I. Sadreyev, P. I. Wang, M. Y. Tolstorukov and R. E. Kingston, The long noncoding RNAs NEAT1 and MALAT1 bind active chromatin sites., *Mol. Cell*, 2014, **55**(5), 791–802.

6 B. L. Gudenas and L. Wang, Prediction of LncRNA subcellular localization with deep learning from sequence features., *Sci. Rep.*, 2018, **8**(1), 16385.

7 M. C. Bridges, A. C. Daulagala and A. Kourtidis, LNCcation: lncRNA localization and function., *J. Cell Biol.*, 2021, **220**(2), e202009045.

8 N. K. Conrad, The emerging role of triple helices in RNA biology, *WIREs RNA*, 2014, **5**(1), 15–29.

9 A. Donlic, M. Zafferani, G. Padroni, M. Puri and A. E. Hargrove, Regulation of MALAT1 triple helix stability and in vitro degradation by diphenylfurans., *Nucleic Acids Res.*, 2020, **48**(14), 7653–7664.

10 F. A. Abulwerdi, W. Xu, A. A. Ageeli, M. J. Yonkunas, G. Arun, H. Nam, J. S. Schneekloth Jr., T. K. Dayie, D. Spector, N. Baird and S. F.-J. Le Grice, Selective small-molecule targeting of a triple helix encoded by the long noncoding RNA, MALAT1., *ACS Chem. Biol.*, 2019, **14**(2), 223–235.

11 A. Donlic, B. S. Morgan, J. L. Xu, A. Liu, C. Roble Jr. and A. E. Hargrove, Discovery of small molecule ligands for MALAT1 by tuning an RNA-binding scaffold., *Angew. Chem., Int. Ed.*, 2018, **57**(40), 13242–13247.

12 M. Zafferani and A. E. Hargrove, Small molecule targeting of biologically relevant RNA tertiary and quaternary structures., *Cell Chem. Biol.*, 2021, **28**(5), 594–609.

13 A. Das, K. Bhadra and G. Suresh Kumar, Targeting RNA by small molecules: Comparative structural and thermodynamic aspects of aristololactam-β-D-glucoside and daunomycin binding to tRNAphe., *PLoS One*, 2011, **6**(8), e23186.

14 H. Yu, W. Yang, O. Alkhamis, J. Canoura, K.-A. Yang and Y. Xiao, In vitro isolation of small-molecule-binding aptamers with intrinsic dye-displacement functionality., *Nucleic Acids Res.*, 2018, **46**(8), e43.

15 J. E. Sokoloski and P. C. Bevilacqua, Analysis of RNA folding and ligand binding by conventional and high-throughput calorimetry., *Methods Mol. Biol.*, 2012, **905**, 145–174.

16 R. Silvers, H. Keller, H. Schwalbe and M. Hengesbach, Differential scanning fluorimetry for monitoring RNA stability., *ChemBioChem*, 2015, **16**(7), 1109–1114.

17 M. M. Fay, S. M. Lyons and P. Ivanov, RNA G-quadruplexes in biology: Principles and molecular mechanisms., *J. Mol. Biol.*, 2017, **429**(14), 2127–2147.

18 C. K. Kwok, G. Marsico and S. Balasubramanian, Detecting RNA G-Quadruplexes (rG4s) in the Transcriptome., *Cold Spring Harbor Perspect. Biol.*, 2018, **10**(7), a032284.

19 C. K. Kwok and S. Balasubramanian, Targeted Detection of G-Quadruplexes in Cellular RNAs., *Angew. Chem., Int. Ed.*, 2015, **54**(23), 6751–6754.

20 J. Jamroskovic, I. Obi, A. Movahedi, K. Chand, E. Chorell and N. Sabouri, Identification of putative G-quadruplex DNA structures in S. pombe genome by quantitative PCR stop assay., *DNA Repair*, 2019, **82**, 102678.

21 X. Yang, J. Cheema, Y. Zhang, H. Deng, S. Duncan, M. I. Umar, J. Zhao, Q. Liu, X. Cao, C. K. Kwok and Y. Ding, RNA G-quadruplex structures exist and function *in vivo* in plants., *Genome Biol.*, 2020, **21**(1), 226.

22 Y. Katsuda, S.-i Sato, L. Asano, Y. Morimura, T. Furuta, H. Sugiyama, M. Hagihara, M. Uesugi and A. Small, Molecule that represses translation of G-quadruplex-containing mRNA., *J. Am. Chem. Soc.*, 2016, **138**(29), 9037–9040.

23 J. A. Brown, M. L. Valenstein, T. A. Yario, K. T. Tycowski and J. A. Steitz, Formation of triple-helical structures by the 3′-end sequences of MALAT1 and MENβ noncoding RNAs, *Proc. Natl. Acad. Sci. U. S. A.*, 2012, **109**(47), 19202–19207.

24 J. A. Brown, D. Bulkley, J. Wang, M. L. Valenstein, T. A. Yario, T. A. Steitz and J. A. Steitz, Structural insights into the stabilization of MALAT1 noncoding RNA by a bipartite triple helix., *Nat. Struct. Mol. Biol.*, 2014, **21**(7), 633–640.

25 T. Gutschner, M. Hämmerle, M. Eissmann, J. Hsu, Y. Kim, G. Hung, A. Revenko, G. Arun, M. Stentrup, M. Gross, M. Zörnig, A. R. MacLeod, D. L. Spector and S. Diederichs,

The noncoding RNA MALAT1 is a critical regulator of the metastasis phenotype of lung cancer cells., *Cancer Res.*, 2013, **73**(3), 1180–1189.

26 T. Gutschner, M. Hämmerle, M. Eißmann, J. Hsu, Y. Kim, G. Hung, A. Revenko, G. Arun, M. Stentrup, M. Groß, M. Zörnig, A. R. MacLeod, D. L. Spector and S. Diederichs, The noncoding RNA MALAT1 is a critical regulator of the metastasis phenotype of lung cancer cells, *Cancer Res.*, 2013, **73**(3), 1180–1189.

27 I. Manfredonia and D. Incarnato, Structure and regulation of coronavirus genomes: State-of-the-art and novel insights from SARS-CoV-2 studies, *Biochem. Soc. Trans.*, 2021, **49**(1), 341–352.

28 C. P. Jones and A. R. Ferré-D'Amaré, Crystal structure of the severe acute respiratory syndrome coronavirus 2 (SARS-CoV-2) frameshifting pseudoknot., *RNA*, 2022, **28**(2), 239–249.

29 P. R. Bhatt, A. Scaiola, G. Loughran, M. Leibundgut, A. Kratzel, R. Meurs, R. Dreos, K. M. O'Connor, A. McMillan and J. W. Bode, Structural basis of ribosomal frameshifting during translation of the SARS-CoV-2 RNA genome., *Science*, 2021, **372**(6548), 1306–1313.

30 A. E. Firth and I. Brierley, Non-canonical translation in RNA viruses., *J. Gen. Virol.*, 2012, **93**(7), 1385–1409.

31 J. E. Wilusz, C. K. JnBaptiste, L. Y. Lu, C. D. Kuhn, L. Joshua-Tor and P. A. Sharp, A triple helix stabilizes the 3′ ends of long noncoding RNAs that lack poly(A) tails., *Genes Dev.*, 2012, **26**(21), 2392–2407.

32 C. E. Hajdin, S. Bellaousov, W. Huggins, C. W. Leonard, D. H. Mathews and K. M. Weeks, Accurate SHAPE-directed RNA secondary structure modeling, including pseudoknots., *Proc. Natl. Acad. Sci. U. S. A.*, 2013, **110**(14), 5498–5503.

33 K. A. Wilkinson, E. J. Merino and K. M. Weeks, Selective 2′-hydroxyl acylation analyzed by primer extension (SHAPE): Quantitative RNA structure analysis at single nucleotide resolution, *Nat. Protoc.*, 2006, **1**(3), 1610–1616.

34 B. Zhang, Y. S. Mao, S. D. Diermeier, I. V. Novikova, E. P. Nawrocki, T. A. Jones, Z. Lazar, C.-S. Tung, W. Luo, S. R. Eddy, K. Y. Sanbonmatsu and D. L. Spector, Identification and characterization of a class of MALAT1-like genomic loci., *Cell Rep.*, 2017, **19**(8), 1723–1738.

35 M. Troutman, The Significance of Early Ct's – Ask TaqMan. **https://www.thermofisher.com/blog/behindthebench/the-significance-of-early-cts-ask-taqman-35/**.

36 C. G.-B. Caraguel, H. Stryhn, N. Gagné, I. R. Dohoo and K. L. Hammell, Selection of a cutoff value for real-time polymerase chain reaction results to fit a diagnostic Purpose: Analytical and epidemiologic approaches., *J. Vet. Diagn. Invest.*, 2011, **23**(1), 2–15.

37 S. I. Omar, M. Zhao, R. V. Sekar, S. A. Moghadam, J. A. Tuszynski and M. T. Woodside, Modeling the structure of the frameshift-stimulatory pseudoknot in SARS-CoV-2 reveals multiple possible conformers., *PLoS Comput. Biol.*, 2021, **17**(1), e1008603.

38 W. D. Penn, H. R. Harrington, J. P. Schlebach and S. Mukhopadhyay, Regulators of viral frameshifting: More than RNA influences translation events., *Annu. Rev. Virol.*, 2020, **7**(1), 219–238.

39 E. P. Plant and J. D. Dinman, The role of programmed-1 ribosomal frameshifting in coronavirus propagation., *Front. Biosci.*, 2008, **13**, 4873–4881.

40 A. E. Firth, B. Y.-W. Chung, M. N. Fleeton and J. F. Atkins, Discovery of frameshifting in Alphavirus 6 K resolves a 20 year enigma., *Virol. J.*, 2008, **5**(1), 108.

41 T. Jacks and H. E. Varmus, Expression of the Rous sarcoma virus pol gene by ribosomal frameshifting., *Science*, 1985, **230**(4731), 1237–1242.

42 R. J. Riegger and N. Caliskan, Thinking outside the frame: Impacting genomes capacity by programmed ribosomal frameshifting., *Front. Mol. Biosci.*, 2022, 9.

43 I. Brierley, S. Pennell and R. J.-C. Gilbert, Viral RNA pseudoknots: Versatile motifs in gene expression and replication., *Nat. Rev. Microbiol.*, 2007, **5**(8), 598–610.

44 E. P. Plant, R. Rakauskaitė, D. R. Taylor and J. D. Dinman, Achieving a golden mean: Mechanisms by which coronaviruses ensure synthesis of the correct stoichiometric ratios of viral proteins., *J. Virol.*, 2010, **84**(9), 4330–4340.

45 D. B. Ritchie, J. Soong, W. K.-A. Sikkema and M. T. Woodside, Anti-frameshifting ligand reduces the conformational plasticity of the SARS virus pseudoknot., *J. Am. Chem. Soc.*, 2014, **136**(6), 2196–2199.

46 K. Zhang, I. N. Zheludev, R. J. Hagey, R. Haslecker, Y. J. Hou, R. Kretsch, G. D. Pintilie, R. Rangan, W. Kladwang, S. Li, M. T.-P. Wu, E. A. Pham, C. Bernardin-Souibgui, R. S. Baric, T. P. Sheahan, V. D'Souza, J. S. Glenn, W. Chiu and R. Das, Cryo-EM and antisense targeting of the 28 kDa frameshift stimulation element from the SARS-CoV-2 RNA genome., *Nat. Struct. Mol. Biol.*, 2021, **28**(9), 747–754.

47 Y. Sun, L. Abriola, R. O. Niederer, S. F. Pedersen, M. M. Alfajaro, V. S. Monteiro, C. B. Wilen, Y.-C. Ho, W. V. Gilbert, Y. V. Surovtseva, B. D. Lindenbach and J. U. Guo, Restriction of SARS-CoV-2 replication by targeting programmed −1 ribosomal frameshifting., *Proc. Natl. Acad. Sci. U. S. A.*, 2021, **118**(26), e2023051118.

48 S. Munshi, K. Neupane, S. M. Ileperuma, M. T.-J. Halma, J. A. Kelly, C. F. Halpern, J. D. Dinman, S. Loerch and M. T. Woodside, Identifying inhibitors of −1 programmed ribosomal frameshifting in a broad spectrum of coronaviruses, *Viruses*, 2022, **14**(2), 177.

49 D.-G. Ahn, G. Y. Yoon, S. Lee, K. B. Ku, C. Kim, K.-D. Kim, Y.-C. Kwon, G.-W. Kim, B.-T. Kim, S.-J. Kim and A. Novel, Frameshifting inhibitor having antiviral activity against zoonotic coronaviruses, *Viruses*, 2021, **13**(8), 1639.